Bioinspiration & Biomimetics

PAPER

Burst-and-coast swimming is not always energetically beneficial in fish (*Hemigrammus bleheri*)

Intesaaf Ashraf[1,*], **Sam Van Wassenbergh**[2,3] and **Siddhartha Verma**[4,5]

[1] Laboratoire de Physique et Mecanique des Milieux Heterogenes (PMMH), CNRS UMR 7636, ESPCI Paris, Universite Paris Diderot, Paris, France
[2] Laboratory of Functional Morphology, University of Antwerp, Belgium
[3] Departement Adaptations du Vivant, UMR 7179, C.N.R.S/M.N.H.N., Paris, France
[4] Department of Ocean and Mechanical engineering, Florida Atlantic University, Boca Raton, FL 33431, United States of America
[5] Harbor Branch Oceanographic Institute, Florida Atlantic University, Fort Pierce, FL 34946, United States of America
[*] Author to whom any correspondence should be addressed.

E-mail: intesaaf.ashraf15@gmail.com

RECEIVED
2 April 2020

REVISED
9 August 2020

ACCEPTED FOR PUBLICATION
3 September 2020

PUBLISHED
3 November 2020

Keywords: fish swimming, intermittent locomotion, burst and coast swimming, flow sensing, energy efficiency

Supplementary material for this article is available online

Abstract

Burst-and-coast swimming is an intermittent mode of locomotion used by various fish species. The intermittent gait has been associated with certain advantages such as stabilizing the visual field, improved sensing ability, and reduced energy expenditure. We investigate burst-coast swimming in rummy nose tetra fish (*Hemigrammus bleheri*) using a combination of experimental data and numerical simulations. The experiments were performed in a shallow water channel where the tetra fish swam against an imposed inflow. High speed video recordings of the fish were digitized to extract the undulatory kinematics at various swimming speeds. The kinematics data were then used in Navier–Stokes simulations to prescribe the undulatory motion for three-dimensional geometrical models of the fish. The resulting steady-state speeds of the simulated self-propelled swimmers agree well with the speeds observed experimentally. We examine the power requirements for various realistic swimming modes, which indicate that it is possible to use continuous swimming gaits that require considerably less mechanical energy than intermittent burst-coast modes at comparable speeds. The higher energetic cost of burst-coast swimming suggests that the primary purpose of intermittent swimming may not be to conserve energy, but it may instead be related to a combination of other functional aspects such as improved sensing and the likely existence of a minimum tail-beat frequency. Importantly, using sinusoidal traveling waves to generate intermittent and continuous kinematics, instead of using experiment-based kinematics, results in comparable power requirements for the two swimming modes.

1. Introduction

Intermittent locomotion is a widely occurring phenomenon that is employed frequently by various animals [1–3]. Intermittent swimming in fish is referred to as burst-and-coast swimming [4], and involves a few flicks of the fish's tail followed by an unpowered glide. One of the primary functions of burst-coast swimming is to enhance sensory capabilities [5–8], where the gliding phase minimizes self-generated 'noise' in the boundary layer on the body. This allows signals of external origin to permeate through to the sensory organ called the lateral line [9]. For instance, the burst-and-coast strategy is observed in blind cave fish, where they accelerate and glide past unfamiliar objects and obstacles repeatedly [10]. This allows them to form a 'hydrodynamic image' of their surroundings by perceiving reflected pressure pulses generated by their motion. Intermittent swimming has also been shown to be critical for avoiding collisions when blind fish approach a solid wall [5, 6].

In addition to stabilizing the sensory field, the inactive phase of intermittent motion is attributed with enhancing the possibility of prey-detection, and diminishing the wake-signature to avoid alerting potential prey and predators [11]. Burst-and-coast

swimming has also been hypothesized to yield energetic benefits [1, 3, 12, 13]. Weihs [12] used simplified analytical approximations to argue that burst-and-coast swimming could reduce energy expenditure by as much as 50 percent, when compared to continuous swimming at the same average speed. These models were further adapted for high speed swimming of cod and saithe by Videler and Weihs [13]. In related work, Blake [14] represented swimming fish as prolate spheroids, and used a simple hydromechanical model to determine that an optimal fineness ratio of approximately 5 was required for maximum energetic benefit of burst-coast swimming. In addition to such analytical approaches, burst-and-coast swimming has been analyzed using simplified experimental [15] and numerical [17] models. Floryan *et al* [15] experimentally investigated a 2D rigid airfoil held on a sting, pitching intermittently about its leading edge. They observed that both the thrust and power increased with increasing duty cycle. Importantly, they surmised that if metabolic energy losses were considered, continuous swimming may be preferable to burst-and-coast motion. Akoz *et al* [16] also investigated pitching airfoils using both viscous and inviscid two-dimensional numerical simulations. Chung [17] performed two-dimensional numerical simulations showing energy savings associated with burst-and-coast swimming, and attributed this to differences in the wake structure between burst-coast and continuous swimming. Dai *et al* [18] used simulations of elastically deforming beams to determine that cost-savings for intermittent swimming depend on the Reynolds number and the duty cycle. Wu *et al* [19] studied the kinematics and wakes of a koi carp (*Cyprinus carpio* koi) and estimated an energy saving of approximately 45% during burst-coast swimming compared to continuous swimming. Several other studies have also investigated burst-and-coast swimming [20–24] and there is consensus in the literature that one of the primary reasons fish employ this intermittent mode is to save energy. We note that the majority of these studies have relied on simplified theoretical models, inviscid numerical computations, two-dimensional Navier–Stokes simulations, or analytical representations of intermittent kinematics, which may limit their applicability to realistic scenarios involving live fish.

In this paper, we investigate burst-coast swimming in rummy nose tetra fish (*Hemigrammus bleheri*) using a combination of experiments and direct numerical simulations. The undulatory kinematics of the fish are extracted from the experiments for various swimming modes, and used in simulations to prescribe the body undulations. The simulated three-dimensional swimmers are entirely self-propelled with no imposed inflow. The experimental setup and numerical methods used are described in section 2. The results for tail-beat duration, steady-state speed, and power requirement for various swimming modes are presented in section 3, followed by a brief discussion and conclusion in section 4.

2. Materials and methods

2.1. Experimental setup and midline discretization

The experimental setup consists of a shallow water channel, where an inflow is imposed at controlled speeds, and the rummy nose tetra fish (*Hemigrammus bleheri*) swim against the flow [25–28]. The detailed experimental protocol is available in reference [27]. The average size of the fish used is: length $\sim$3.5 cm, width $\sim$0.4 cm and height $\sim$0.4 cm–0.5 cm. The fish were housed in an aquarium tank at a temperature between 26°C–27°C, and fed six times per week. The experiments were carried out at the same temperature, in a water channel with a test section of depth 2.2 cm and a swimming area of 20 cm $\times$ 50 cm. The turbulence intensity was found to be below 2% and it was independent of the flow rate in the test section. The fish were observed to use the intermittent burst-and-coast swimming mode a majority of the time while swimming at normalized speeds below 2 body lengths per second. Beyond this speed, the tendency of using continuous strokes increased at higher flow speeds, and the intermittent mode was used less frequently.

To extract the kinematics of the fish's body midline, high frame rate video recordings of the swimming tetra fish (400 Hz) were segmented, and the corresponding midlines were digitized for each frame. The digitized midlines were then post-processed to remove frame jitter by averaging over 9 frames, and minor segmentation errors that led to small variations in the total length of the midline were fixed. These procedures helped ensure a smoother transition between frames, and helped keep the total body length of the fish constant over the course of the simulation. After initial cleanup, interpolating cubic splines were fitted through the midline datapoints for each of the frames, and the resulting coefficients were stored for use by the Navier–Stokes solver. The spline interpolation was done using 9 piecewise segments, with the corresponding knot locations given as follows:

$$(s_0, \ldots s_i, \ldots, s_9)/L = (0, 0.1, 0.2, 0.35, 0.5, 0.65, \times 0.75, 0.85, 0.93, 1) \quad (1)$$

Here, s represents the curvilinear coordinate along the midline, starting at the head and terminating at the tail end, and L is the total length of the fish. The Navier–Stokes solver uses the resulting coefficients to reconstruct the cubic spline at the appropriate time steps. If the simulation time step lies in between two available frames, linear interpolation is used to determine the corresponding midline shape.

2.2. Numerical methods

The simulations used in this work are based on the three-dimensional incompressible Navier–Stokes equations:

$$\nabla \cdot \mathbf{u} = 0 \tag{2}$$

$$\frac{\partial \mathbf{u}}{\partial t} + \mathbf{u} \cdot \nabla \mathbf{u} = -\frac{\nabla p}{\rho} + \nu \nabla^2 \mathbf{u} + \lambda \chi (\mathbf{u}_s - \mathbf{u}) \tag{3}$$

Solid objects, i.e., the swimming fish, are represented on the computational grid via the characteristic function χ, and interact with the fluid by means of the penalty term $\lambda\chi(\mathbf{u}_s - \mathbf{u})$ [29]. The penalty parameter is set to $\lambda = 1/dt$, where dt is the time-step size determined at each step using the Courant–Friedrichs–Lewy condition. In equation (3), $\mathbf{u}_s$ denotes the swimmer's combined translational ($\mathbf{u}_{\mathrm{CM}}$), rotational, and deformation velocity ($\mathbf{u}_{\mathrm{Def}}$), whereas $\mathbf{u}$ and ν correspond to the fluid velocity and viscosity, respectively. p represents the pressure, and ρ represents the density of both the fluid and the solid, since we assume neutrally buoyant fish. The deformation velocity $\mathbf{u}_{\mathrm{Def}}$ is prescribed using the midline kinematics extracted from the controlled experiments. Additional details regarding the geometric shape of the swimmer and the prescribed swimming kinematics are provided in the appendices A and B.

We use the pressure-projection method [30] and finite differences for solving the Navier–Stokes equations using the CUBISM software framework [31], which has been used in previous work for investigating groups of swimmers [32]. We note that prescribing the midline kinematics leads to slight variations in the volume of the fish, with the maximum observed deviation being approximately 0.16%. This happens because the curvilinear length of the midline is fixed at the chosen L, and as the body bends there can be a small overlap among grid points on the concave side. This non-divergence-free deformation of the self-propelled swimmers is incorporated into the pressure-Poisson equation as follows:

$$\nabla^2 p = \frac{\rho}{\Delta t} \left(\nabla \cdot \mathbf{u}^\star - \chi \nabla \cdot \mathbf{u}_s \right), \tag{4}$$

where $\mathbf{u}^\star$ represents the intermediate velocity from the convection–diffusion-penalization fractional steps. Equation (4) was solved using the fast fourier transform on uniform grids. All of the simulations employ grids with $1024 \times 512 \times 512$ points along the three dimensions, and domains of size $1 \times 0.5 \times 0.5$ units. Increasing the grid resolution to twice these values in each direction showed no appreciable change in the swimming speed of the fish. The length of the swimmers was set to be 0.2 units, which corresponds to approximately 200 grid points along the length of the fish.

2.3. Flow-induced forces and energetics

The pressure-induced and viscous forces acting on the swimmers are computed as follows [32]:

$$\mathbf{dF}_p = -p\mathbf{n}\, dS \tag{5}$$

$$\mathbf{dF}_\nu = 2\mu \mathbf{D} \cdot \mathbf{n}\, dS \tag{6}$$

Here, p represents the pressure acting on the swimmer's surface, $\mathbf{D} = \left(\nabla \mathbf{u} + \nabla \mathbf{u}^{\mathrm{T}}\right)/2$ is the strain-rate tensor on the surface, and dS denotes the infinitesimal surface area. The vector $\mathbf{n}$ represents the local surface normal, and μ is the dynamic viscosity. Equations (5) and (6) provide local force vectors at each grid point that is part of the swimmer's body surface. Since self-propelled swimmers generate zero net average force during steady swimming, we determine the instantaneous thrust as follows [33]:

$$\mathrm{Thrust} = \frac{1}{2\|\mathbf{u}_{\mathrm{CM}}\|} \iint \left(\mathbf{u}_{\mathrm{CM}} \cdot \mathbf{dF} + |\mathbf{u}_{\mathrm{CM}} \cdot \mathbf{dF}| \right), \tag{7}$$

where $\mathbf{dF} = \mathbf{dF}_p + \mathbf{dF}_\nu$, and the double-integrals represent surface-integration over the swimmer's body. Here, $\mathbf{u}_{\mathrm{CM}}$ is the instantaneous center-of-mass velocity, i.e., the translational velocity of the fish, and the norm in the denominator represents its magnitude. Similarly, the instantaneous drag may be determined as:

$$\mathrm{Drag} = \frac{1}{2\|\mathbf{u}_{\mathrm{CM}}\|} \iint \left(\mathbf{u}_{\mathrm{CM}} \cdot \mathbf{dF} - |\mathbf{u}_{\mathrm{CM}} \cdot \mathbf{dF}| \right) \tag{8}$$

These definitions project the force vector at each surface grid point along the direction of the translational velocity; positive contributions become part of the instantaneous thrust (equation (7)), whereas negative values contribute to instantaneous drag (equation (8)). Over a full periodic cycle during steady swimming, the time average of the thrust from equation (7) will be equal to the time average of the drag from equation (8), since the average acceleration is zero.

Using these definitions, the instantaneous thrust- and deformation-power are computed as:

$$P_{\mathrm{Thrust}} = \mathrm{Thrust} \cdot \|\mathbf{u}_{\mathrm{CM}}\| \tag{9}$$

$$P_{\mathrm{Def}} = -\iint \mathbf{u}_{\mathrm{Def}} \cdot \mathbf{dF}, \tag{10}$$

where $\mathbf{u}_{\mathrm{Def}}$ represents the deformation-velocity of the swimmer's body, i.e., the undulation velocity at each surface grid point, computed in the center-of-mass reference frame. The average swimming-efficiency is then computed based on a modified form of the Froude efficiency proposed in reference [34]:

$$\eta = \frac{\int_{t_1}^{t_2} P_{\mathrm{Thrust}}\, dt}{\int_{t_1}^{t_2} P_{\mathrm{Thrust}}\, dt + \int_{t_1}^{t_2} \max(P_{\mathrm{Def}}, 0)\, dt}, \tag{11}$$

whereas the cost of transport (CoT) is defined as:

$$\mathrm{CoT}(t) = \frac{\int_{t_1}^{t_2} \max(P_{\mathrm{Def}}, 0)dt}{\int_{t_1}^{t_2} \|\mathbf{u}_{\mathrm{CM}}\|dt} \tag{12}$$

The limits t_1 and t_2 are selected such that they include at least one full tail-beat cycle during continuous swimming, or one full burst-coast cycle during intermittent swimming. To compute both η and the CoT, we do not consider negative values of P_{Def}. This restriction yields conservative estimates for both η and the CoT, and accounts for the fact that the elastically rigid simulated swimmers may not store any mechanical energy provided by the flow. All CoT values reported in this study have been normalized by the weight of the fish.

3. Results

3.1. Burst-and-coast kinematics

The tetra fish (*Hemigrammus bleheri*) in the shallow water tunnel with controlled flow rates were observed to spontaneously adopt a station-holding behaviour while swimming against the flow. Using high frame rate video recordings, we observed that the fish use a burst-and-coast swimming gait over the whole range of swimming speeds tested. At high speeds, the coasting time is reduced greatly so that the kinematics can be described fairly well by a single tail-beating frequency, as has been considered in recent studies describing collective swimming in similar experimental configurations [25, 26].

The midline kinematics and the time variation of the tail-beat amplitude at the rear end of the caudal fin are shown in figure 1 for three different swimming speeds. The burst-and-coast dynamics can be clearly observed; during each swimming bout of duration T_{p}, the tail moves actively during the bursting time T_{b}, and then remains motionless for coasting time T_{c}, after which a new bout starts with the next burst. From the A_r plots in figure 1 we also observe that at low swimming speeds the burst consists of only a half tail-beat, which is related to the clear asymmetry observed in the midline kinematics shown in the figure. We refer to this as the half tail-beat mode or 'HT' mode [19]. The fish respond to an increase in inflow velocity by increasing the burst period, which allows them to swim faster as shown in figure 2. However, after a certain velocity the fish can no longer maintain the HT mode, and switch to the multiple tail-beat ('MT') mode. The first MT scenario involves a full back and forth tail-beat for every burst event, followed by a coasting period. Subsequently, for even higher velocities, multiple tail-beats occur per burst followed by a very short coasting period. This is as an MT mode as well, albeit given the extremely long burst duration, the fish appear to be swimming continuously. Thus, we also refer to the last multiple tail-beat mode as 'continuous' swimming in this work. The total bout period in this case is the sum of the multiple burst periods and the final coast period.

3.2. Navier–Stokes simulations

Tail-beat kinematics from the three different swimming modes (HT-, MT-, and continuous-mode) were discretized, similar to the midline time-lapses shown in figure 1, and incorporated into Navier–Stokes simulations of swimming fish. We use a simplified three-dimensional model representation of the tetra fish, and time-varying undulations along the spine (midline) of the model are imposed directly from the kinematics recorded during the experiments. Figure 3 shows flow structures that develop in the wakes for the three different cases: the HT mode where the fish employs one-sided asymmetric burst-coast motion; the MT mode where it coasts after every complete tail-beat cycle; and the continuous mode where it swims for relatively long periods followed by short coasts. The corresponding animations are available in supplementary movies 2 to 4. The Reynolds numbers ($\mathrm{Re} = UL/\nu$) for these three cases are 640, 1840, and 5900, respectively.

In figure 3(a), we observe an asymmetry in the wake structure which is related to the one-sided nature of the midline envelope for the HT mode. The asymmetric kinematics will eventually cause the fish to yaw, and the fish changes its tail beat direction at some point to prevent this from happening (figure 1(a) and movies 1 and 2). This allows the fish to continue swimming in a straight line. We note that the wake signature is limited to a short range, due to quickly diminishing strength of the flow structures downstream of the fish. The weaker wake in the HT mode may be caused by a combination of higher viscous dissipation at the lower Reynolds number, as well as lower absolute power output from the fish. One of the advantages of limiting the extent of the wake is that it avoids alerting potential prey that may be present nearby.

The flow structures for a full MT tail-beat cycle, where the tail flicks once to the right and then to the left before coasting, are shown in figure 3(b). We observe a much more prominent wake, with the vortices arranged in two v-shaped diverging rows. Furthermore, the vortices do not dissipate as quickly compared to those for the HT mode. The wake structure for the continuous swimming mode is shown in figure 3(c), and it also exhibits two diverging rows of vortices in the wake that spread out over a large area and remain strong far downstream of the fish. These vortices could be easily detected by other fish and aquatic animals from afar, which would potentially allow them to identify and follow the wake signature.

The time-varying speeds for the three intermittent swimming cases are shown in figure 4. All three simulated fish start from rest. Initially, an analytical sinusoidal traveling wave is used to describe the undulatory kinematics until the fish reach steady

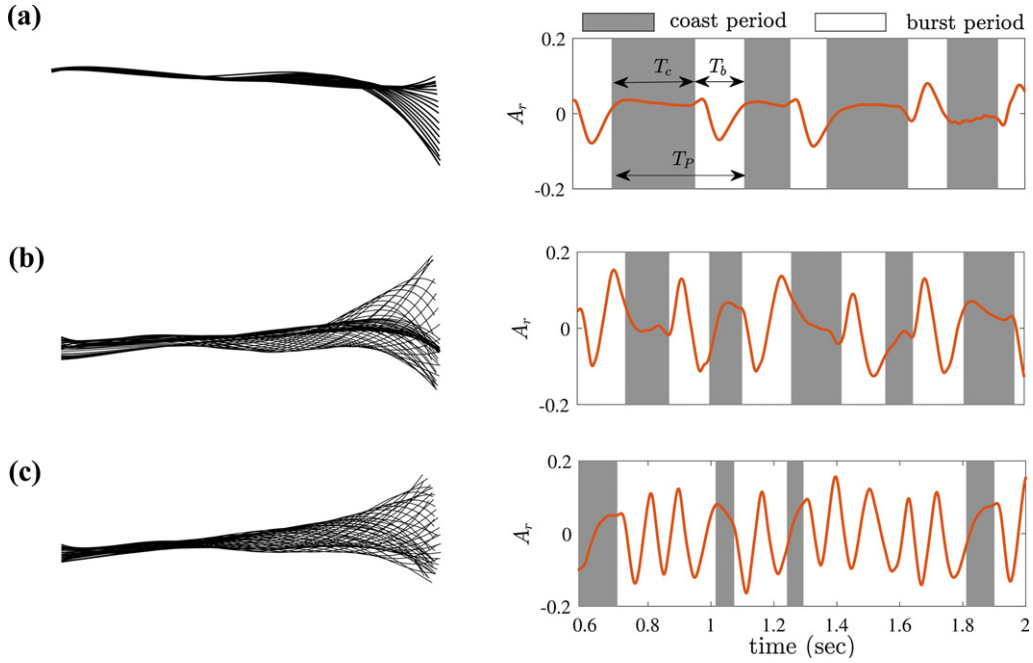

Figure 1. Fish kinematics at various swimming speeds: (a) $U = 0.36$ body lengths per second (BL s^{-1}), (b) $U = 0.87$ BL s^{-1}, (c) $U = 2.69$ BL s^{-1} (figure adapted from [27, 28]). Left column-time lapse of the midline positions of a left-facing fish, where the leading edges have been aligned to lie along the same vertical line. Right column-corresponding excursion of the tail tip. A video of fish swimming with the three different modes shown here is provided in movie 1 (https://stacks.iop.org/BB/16/016002/mmedia). A_r represents the lateral displacement of the posterior end of the caudal fin. We note that the first case involves an asymmetric one-sided tail-beat, whereas the remaining two cases entail complete two-sided cycles. The differences in kinematics depend on the speed of water inflow in the channel. As the fish need to swim faster, they move closer to continuous swimming with progressively smaller coasting periods. We note from figure 1(c), where the swimming speed is the highest, that the fish swims continuously for a while followed by very short deceleration or coasting periods.

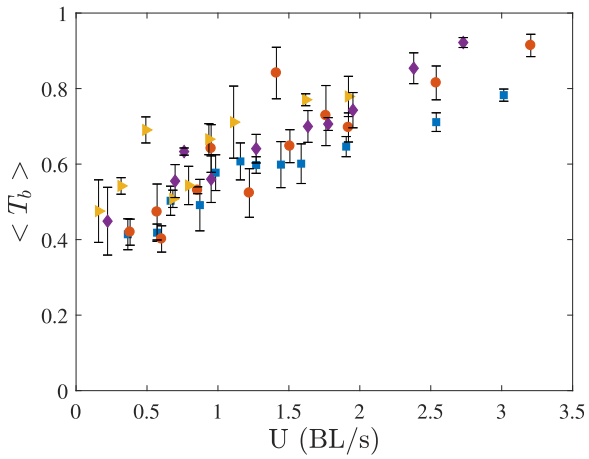

Figure 2. Burst period ratio $< T_b > = T_b(\text{sec})/T_p(\text{sec})$ plotted as a function of swimming velocities, where T_b is the burst period and T_p is the total bout period. Figure adapted from references [27, 28]. The total bout period is the sum of the total burst time, T_b, and the coasting time T_c which follows the burst period. Each color and symbol corresponds to a different fish, meaning that the data shown correspond to 4 different fish used in the study. The error bars indicate the standard deviation. We observe that the fish use longer relative burst periods at higher swimming speeds.

swimming speeds. After attaining steady speed, the undulatory motion is switched over to kinematics extracted from the experimental recordings. This switch is evident as a sudden drop in the three speed curves shown in figure 4. The transition can also be observed in supplementary movies 2 to 4, where the midline shape changes from the sinusoidal description to the experiment-based shape via linear interpolation in time.

After a few burst-coast cycles using the experiment-based kinematics, the swimmers reach a new steady state. The average steady state swimming speeds obtained from the simulations agree well with the experimental values, and this direct correspondence between experimental and simulation data serves as confirmation that our simulations account for the locomotion mechanics correctly. We emphasize that the swimming speeds reported for

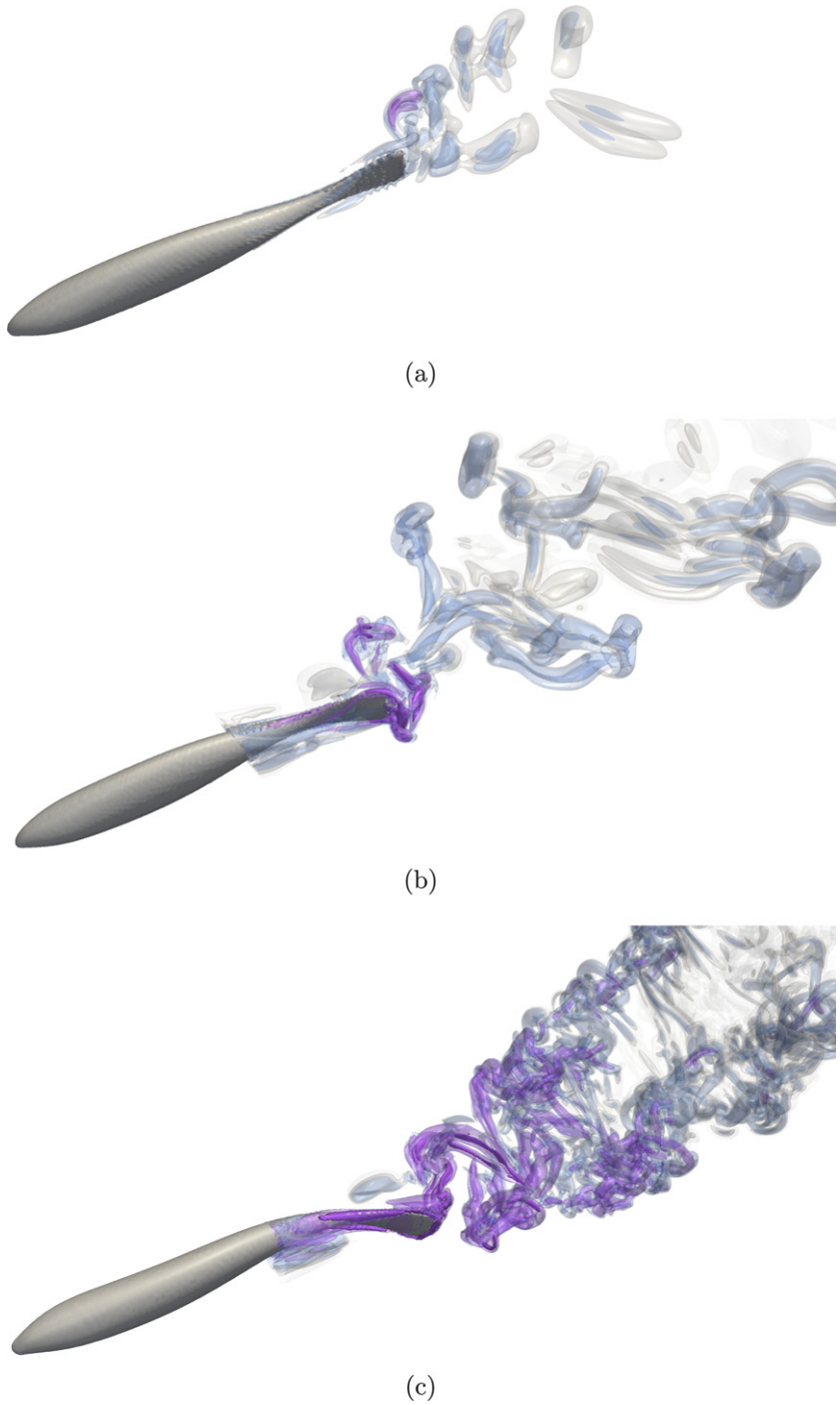

Figure 3. Visualizations of the wake structures for fish swimming at (a) $U = 0.32$ BL s^{-1}, (b) $U = 0.92$ BL s^{-1}, and (c) $U =$ BL s^{-1} (the corresponding animations are available in movies 2–4). The undulation kinematics were imposed from experimental observations for fish swimming at 0.36 BL s^{-1}, 0.87 BL s^{-1}, and 2.69 BL s^{-1}, respectively. We note that the resulting speeds from the Navier–Stokes simulations match the corresponding experimental values to within 11%. The flow-structures have been visualized using contours of the Q-criterion, and they emphasize regions where the flow is predominantly rotational. Darker shades correspond to stronger rotation (vorticity), and lighter shades indicate weaker rotation, primarily in the far-wake region where viscous effects have dissipated the energy contained in the flow.

the Navier–Stokes simulations are outcomes of the simulations; we do not impose an inflow velocity or translational constraints on the fish. The only motion specified a-priori for the fish models are the undulatory kinematics extracted from the experiments. Furthermore, the fish are allowed to yaw freely as can be observed in movies 2–4. However, the roll and pitch rotations are locked due to the absence of control surfaces that can correct for deviations along these axes. As expected, the three different swimming modes give rise to markedly different steady state speeds.

3.3. Burst-coast vs. continuous swimming

To ensure a fair comparison of energy consumption between burst-coast and continuous swimming, we

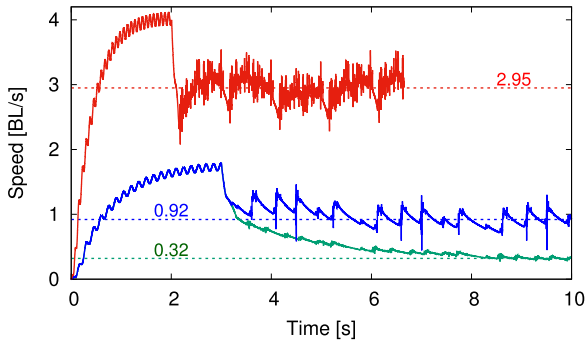

Figure 4. Time-evolution of the fishes' speeds, simulated using the three different swimming modes. The green curve corresponds to the fish employing the HT swimming mode, the blue curve corresponds to the MT mode, and the red curve corresponds to the fish using continuous kinematics (i.e., the MT mode with extremely short coasting durations). We observe that the steady speeds which the simulated fish attain agree well with the experimental values (the corresponding experimental values were 0.36 BL s^{-1}, 0.87 BL s^{-1}, and 2.69 BL s^{-1}, for the three respective cases).

simulated continuously swimming fish at the same steady speeds as those swimming with the intermittent MT and HT modes. This was done by re-using the continuous swimming kinematics from the experimental recordings at 2.69 BL s^{-1}, but by artificially increasing the time interval between the recorded frames. This effectively reduces the continuous tail-beat frequency, thereby reducing the steady speed that the fish can attain. We refer to these as the 'MT-continuous' and the 'HT-continuous' modes. The resulting wake structures and the corresponding time-varying speeds are shown in figure 5. The corresponding animations are available in supplementary movies 5 and 6. In both cases, we observe the diverging row of vortices associated with two-sided tail-beat patterns. The wake of the HT-continuous swimmer (figure 5(a)) dissipates quickly compared to that of the MT-continuous swimmer (figure 5(a)). In figure 5(c), we confirm that the steady-state speeds of the two swimmers are comparable to those of their intermittent counterparts.

3.4. Energetics comparison

We now compare the swimming performances from these five distinct scenarios, i.e., the HT, MT, continuous, HT-continuous, and MT-continuous modes, in figure 6 using a variety of energetics metrics. The metrics discussed here are considered from a purely mechanical viewpoint and do not reflect the total metabolic cost of the animal. For instance, the muscles' energy depletion rates may be contraction-speed dependent, or a muscle system that is tuned evolutionarily for fast escaping performance could be intrinsically more efficient at producing power during shorter and faster muscle contractions. However, these considerations are beyond the scope of the present study.

We observe that going from the HT to MT to continuous swimming mode entails a significant increase in power requirement; the absolute power required for continuous swimming at 2.95 BL s^{-1} is approximately 8.54 times higher than for 0.92 BL s^{-1}, and 15 times higher than for 0.32 BL s^{-1}. This is expected given the notable disparity in swimming speeds. However, when swimming at comparable speeds, the power consumption is markedly lower for continuous gaits compared to intermittent gaits; the HT-continuous mode requires approximately 6% of the power consumed in the HT mode, and the MT-continuous mode requires 50% of the power consumed in the MT mode. For the three continuous swimming modes shown in table 1, the measured power values scale approximately as the cube of the steady state speeds, which is the expected theoretical scaling for these quantities. The CoT (Cost of Transport-which is a 'gallons-per-mile' metric) values for the HT-/MT-continuous modes are notably lower than those for the intermittent HT/MT modes. Likewise, the average swimming efficiencies for the continuous modes are higher than the corresponding burst-and-coast modes. These observations may be related to the fact that abrupt acceleration during the burst phases for the intermittent modes requires considerably more power than the more gradual accelerations experienced during continuous swimming. This can be observed in figure 7, where we compare the time-variation of the speed and power for the intermittent HT mode swimmer and the HT-continuous mode swimmer. The speeds of the two swimmers are comparable, but the coasting phase in the HT mode leads to periodic declines in speed followed by sharp upturns during the burst phases. The comparatively abrupt lateral motion of the midline during the burst phase for the intermittent HT swimmer results in a significantly higher power requirement, as can be observed in figure 7(b).

Focusing on the peaks in speed and power around 6.8 s for the HT mode, we observe that the initial surge in power occurs during the first 'bump' in speed. This corresponds to the sudden initial lateral motion of the tail after the fish has been coasting for a while. By examining the midline kinematics at these times, we determined that the power rises as the caudal fin of the

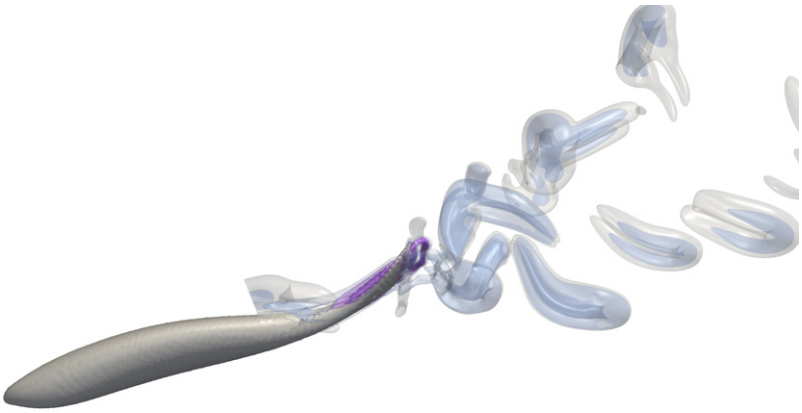

(a)

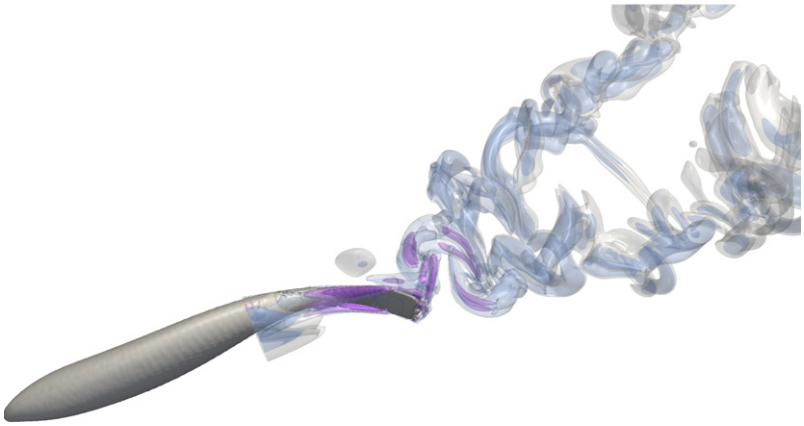

(b)

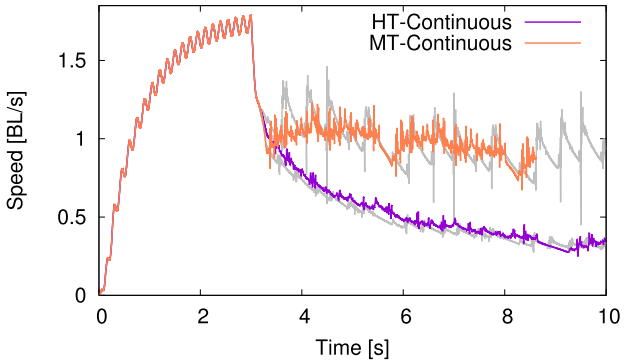

(c)

Figure 5. (a) Visualization of the wake for a fish swimming at $U = 0.40$ BL s^{-1}, but using continuous kinematics (HT-continuous mode). The wake vortices dissipate significantly as they travel downstream. (b) Visualization of the wake for a fish swimming at $U = 0.95$ BL s^{-1}, but using continuous kinematics (MT-continuous mode). The corresponding animations are available in supplementary movies 5 and 6. (c) Time-evolution of the speeds of fish swimming with the HT-continuous and MT-continuous modes. The gray curves in the background correspond to the speeds obtained using the original HT and MT modes (also shown in figure 4). The continuous swimming kinematics from the experimental recordings at 2.69 BL s^{-1} were reused, but after increasing the time step intervals between the recorded frames. The MT-continuous curve corresponds to a simulation where the time step size between the frames was increased to 2.5 times the original value, whereas the HT-continuous curve corresponds to an increase of 6 times the original value.

fish moves outward (increasing lateral displacement) during the half-tail beat. The power starts decreasing from the peak value as the tail starts returning to the straight body pose, and slows down in preparation for the coasting phase. The second 'bump' in speed, which is the maximum for this period, occurs at approximately 6.82 s, while the fin is still returning to the straight coasting pose and its lateral velocity is decreasing.

We note that the CoT and the swimming efficiency do not display similar trends across the 5 cases shown in figure 6. High speed continuous swimming entails

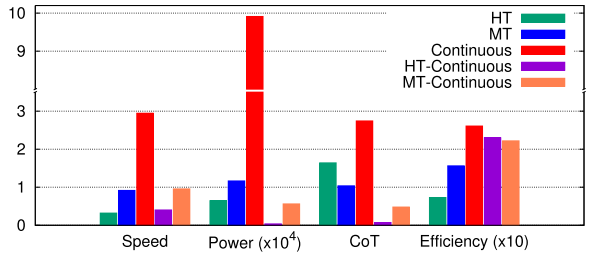

Figure 6. Comparing the energetics performance of five different swimming modes. The corresponding numerical values are provided in table 1, and the metrics have been computed using the definitions described in section 2.3. The power consumption is computed as the average over several burst-coast cycles.

Table 1. Simulation results used to create the energetics plots shown in figure 6. The corresponding definitions can be found in section 2.3.

Swimming mode	Speed (BL s^{-1})	Power (P_{Def})	CoT	Efficiency (%)
HT	0.32	6.46×10^{-5}	1.64	7.3
MT	0.92	1.16×10^{-4}	1.03	15.6
Continuous	2.95	9.91×10^{-4}	2.74	26.1
HT-continuous	0.40	3.61×10^{-6}	0.073	23.0
MT-continuous	0.96	5.62×10^{-5}	0.479	22.2

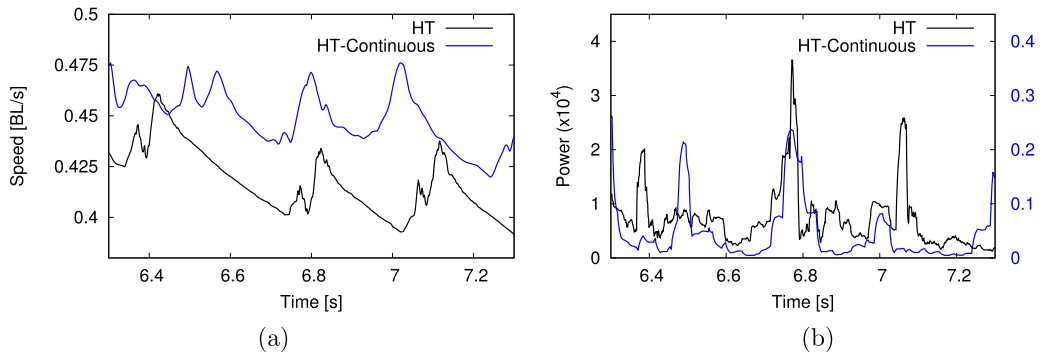

Figure 7. (a) Speed and (b) power comparison for swimmers using the intermittent HT mode and the HT-continuous mode. Note that the scale for the HT-continuous power is an order of magnitude smaller than that for the HT mode, with the corresponding values shown on the right vertical axis. We observe that the power surges correspond to the burst-related peaks in the speed curves, notably at 6.4 s, 6.75 s, and 7.05 s.

the highest CoT (i.e., more energy required per unit distance travelled), while at the same time displaying the highest efficiency. This apparent discrepancy can be explained by considering the respective definitions of the two metrics in equations (11) and (12). The efficiency η considers how much useful thrust power is being generated relative to the deformation power for undulating the body. We expect power values to scale as the cube of the swimming speed, and thus changes that occur in the numerator and the denominator will be comparable. In other words, the high efficiency value for the continuous swimmer at 2.95 BL s^{-1} indicates that although the deformation power required for undulating the body increases substantially, a large amount of useful thrust power is being generated that propels the fish forward by overcoming the substantially larger drag. On the other hand, CoT considers the ratio of deformation power to speed, where the numerator increases substantially faster than the denominator at higher speeds. Thus, for continuous swimming at 2.95 BL s^{-1}, the increase in the required deformation power is significantly higher than the increase in speed, resulting in a high CoT value. Overall, the two metrics offer differing viewpoints of energy usage, and one may be preferable to the other depending on the intended application, which is why we have chosen to report both these values for all the cases considered here.

Overall, the results suggest that if energy-efficiency is the sole concern, continuous swimming may be preferable to intermittent gaits. We point out an important consideration in these comparisons, that the HT-/MT-continuous modes are extrapolations of realistic continuous-swimming behaviour observed at higher speeds to slower speeds. Doing so is necessary since the tetra fish did not exhibit continuous-swimming at low speeds.

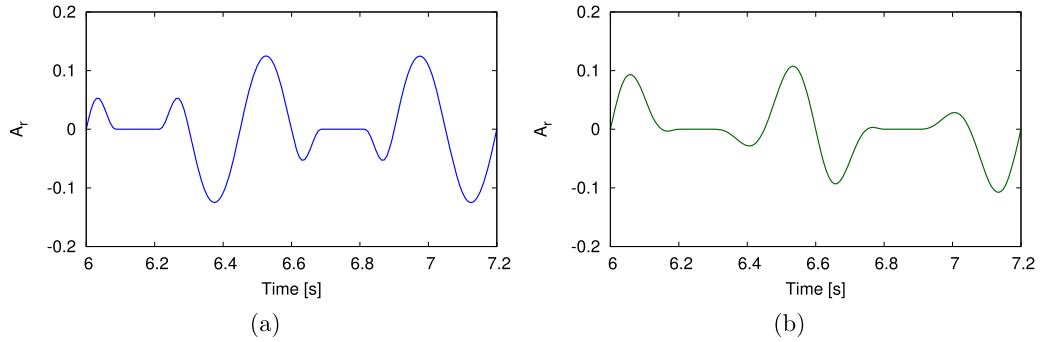

Figure 8. Lateral displacement of the posterior end of the caudal fin for (a) idealized burst-coast case A, and (b) idealized burst-coast case B.

3.5. Burst-coast swimming using idealized kinematics

To further examine the large observed discrepancy in power requirement between continuous and burst-coast swimming, we now consider analytical sinusoidal traveling waves to describe both forms of kinematics:

$$y_{\text{midline}}(s,t) = f(t)\cdot\frac{4}{33}(s+0.031\,25L) \cdot \sin\left(2\pi\left(\frac{s}{L}-\frac{t}{T}\right)+\phi\right) \qquad (13)$$

The function $f(t)$ controls the time-varying envelope of the tail-beat amplitude, ϕ is set to 0, and y_{midline} represents the lateral displacement of the midline in the center-of-mass reference frame. For continuous swimming, $f(t)$ is set to a constant value of 1, whereas for burst-coast swimming it is defined as the following piecewise continuous function [35]:

$$f(t) = \begin{cases} 1 & t \in \Delta t_{\text{steady}} \\ 1-3\lambda_{\text{decel}}^2+2\lambda_{\text{decel}}^3 & t \in \Delta t_{\text{decelerate}} \\ 0 & t \in \Delta t_{\text{coast}} \\ 3\lambda_{\text{accel}}^2-2\lambda_{\text{accel}}^3 & t \in \Delta t_{\text{accelerate}} \end{cases} \qquad (14)$$

Here, $\lambda_{\text{decel}}, \lambda_{\text{decel}} \in [0,1]$ are ramp functions increasing linearly from 0 to 1 during the transition periods $\Delta t_{\text{decelerate}}$ and $\Delta t_{\text{accelerate}}$, respectively. The various time intervals in equation (14) denote: the short time for which the fish beats its tail in a burst-coast cycle (Δt_{steady}); the time it takes the fish to decelerate to the coasting phase ($\Delta t_{\text{decelerate}}$); the time for coasting (Δt_{coast}); and the time required for accelerating back up to the steady phase ($\Delta t_{\text{accelerate}}$).

To represent continuous swimming for the comparison, we set the tail-beat time period to $T = 0.4$ in equation (13), with $f(t) = 1$. For the idealized burst-coast scenario, we use two different kinematics that lead to similar speeds: the idealized burst-coast case A with $T = 0.3$, $\Delta t_{\text{steady}} = 0.3$, $\Delta t_{\text{decelerate}} = 3/35$, $\Delta t_{\text{coast}} = 9/70$, and $\Delta t_{\text{accelerate}} = 3/35$; and idealized burst-coast case B with $T = 0.3$, $\Delta t_{\text{steady}} = 0$, $\Delta t_{\text{decelerate}} = 0.2$, $\Delta t_{\text{coast}} = 0.1$, and $\Delta t_{\text{accelerate}} = 0.3$. The time intervals for case A have been proportioned according to kinematics observed from live tetra fish, whereas the values for case B have been selected manually to yield smooth acceleration and deceleration phases. The time variation of the lateral displacements for these two idealized cases is shown in figure 8. We observe that the motion of the fin is more abrupt for case A than for case B. We also note that the tail-beat direction alternates after every coasting phase, which helps to minimize yaw. This is implemented by changing the phase angle ϕ in equation (13) by π radians after every coast.

The resulting speed and power plots are shown in figure 9, where we observe that the three different kinematics result in similar steady-state swimming speeds, and the power requirements are of the same order of magnitude. The average speed, power, CoT, and efficiency values are provided in table 2. We observe that there is a noticeable difference between the two burst-coast cases; gentler acceleration and deceleration in case B result in a substantial reduction in power requirement and CoT compared to case A. We also observe the impact of abrupt motion on the instantaneous power curves in figure 9(b). At approximately 6.2 s, there is a spike in power as the fish from case A starts an abrupt tail-beat at the end of a coasting phase. In comparison, the fish from case B uses a gradual transition from coasting to acceleration at approximately 6.3 s, which reduces power requirement over the full burst-coast cycle, albeit resulting in a lower average speed.

Another noticeable aspect of the instantaneous power curves shown in figure 9(b) is the presence of negative values for the idealized burst-coast cases, but not for the continuous swimming case. Mechanically, this happens during the deceleration phase, when the flow-induced pressure and viscous forces no longer oppose, but instead aid, the body's lateral motion. We reiterate that we do not consider these negative values in our computations of the energetics metrics, and that doing so would further reduce both the average power and CoT for the idealized burst-coast cases. From table 2 we observe that the CoT for

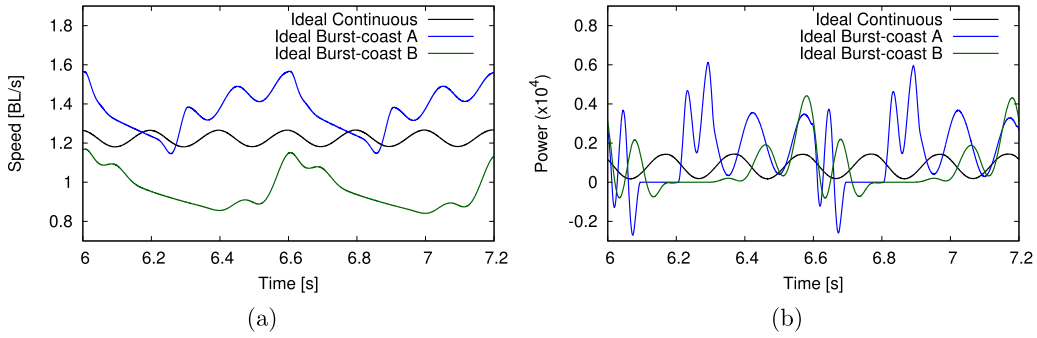

Figure 9. (a) Speed and (b) power comparison for swimmers using idealized continuous kinematics, and idealized burst-and-coast kinematics with two different sets of burst-coast parameters.

Table 2. Simulation results for the swimmers using idealized kinematics.

Swimming mode	Speed (BL s^{-1})	Power (P_{Def})	CoT	Efficiency (%)
Idealized continuous	1.22	8.20×10^{-6}	0.055	42.6
Idealized burst-coast A	1.37	1.59×10^{-5}	0.102	39.3
Idealized burst-coast B	0.96	7.43×10^{-6}	0.070	35.9

case B is comparable to that of the idealized continuous mode. This indicates that it may be feasible to tune the burst-coast parameters to recover idealized kinematics which yield a lower CoT than idealized continuous swimming. This would require an optimization-based study, which is outside the scope of the current work since the focus here is on realistic kinematics extracted from live fish.

4. Discussion and conclusion

The results presented here have crucial implications regarding our current understanding of fish locomotion in nature, and lead us to the following question: why do fish employ burst-and-coast swimming when they could rely on other gaits that are more energy-efficient? There are a number of factors that may determine the answer to this question, which cannot be explored conclusively in the scope of the present study. For instance, it is possible that at lower speeds fish feel increasingly vulnerable to predators, and the need for early-sensing takes precedence over energy-effectiveness; the flow-sensing organs present on fish's bodies (neuromasts) are better able to identify external disturbances during the gliding phase of burst-coast swimming [5–8, 38]. Moreover, comparing the wake structures in figures 3 and 5, we note that continuous swimming leaves behind a well-organized wake that dissipates slowly compared to intermittent swimming at comparable speeds. This would make continually-swimming fish easily detectable by potential predators and prey, which can prove to be detrimental to the fish's well-being.

We remark that we attempted to use particle image velocimetry to measure the power required during burst-coast swimming experimentally. However, these attempts were unsuccessful since the bright laser sheet caused the fish to start swimming randomly, and sometimes even led to their unexplained death. Upon examining our experimental database further, we also realized that the tetra fish do not employ tail-beat frequencies lower than 2 Hz for any given scenario. The existence of a minimum tail-beat frequency appears to be true for several other fish species as well [36, 37]. This presents another potential explanation for the transition from continuous- to MT- to HT-modes; if the fish need to swim at slow steady speeds while maintaining station at a preferred location, it is arguable that being restricted to tail-beat frequencies of 2 Hz or higher will cause them to employ longer coasting durations, and eventually switch to the half-tail-beat mode as observed in the experiments.

Using numerical simulations that employ kinematics extracted from the fish-swimming experiments, we determine that the power requirement for intermittent swimming can be higher than that for certain continuous swimming gaits in tetra fish. This conclusion is in disagreement with the prevalent view that one of the primary functions of burst-coast swimming is to conserve energy. We note that the majority of past studies that have supported this hypothesis have relied on simplified analytical approximations, on inviscid numerical computations, or they have used idealized representations of burst-coast kinematics. Comparing our present work to 2D Navier–Stokes simulations by Chung [17] which demonstrate cost savings in burst-coast swimming, there are certain differences in numerical implementation that could contribute to the differing conclusions, apart from their simulations being two-dimensional. For instance, the 2D simulations do not allow lateral displacement and rotational motion

of the fish, and employ analytical traveling waves to describe continuous swimming as well as burst-coast kinematics. We have demonstrated here that using idealized kinematics in 3D simulations can lead to comparable power requirements for the two swimming modes, but this is not the case when using realistic kinematics extracted from the experiments. Another difference from the two-dimensional study is that their simulations do not exclude negative power values from the energetics estimates, which can manifest in idealized burst-coast swimming during transition to the coasting phase (figure 9). This is an important consideration, especially since the energetic gains observed by Chung were relatively modest at low Re (13.5% at Re = 500), and might disappear altogether when negative power values, if present, are discarded.

We identify other factors that must be considered in the present simulations, such as the impact of averaging the experimental kinematics over multiple frames, which can influence the speed and power required to some extent. Moreover, the effect of body elasticity (i.e., mechanical stiffness) is not accounted for in the current work, and likely plays a role in the swimming energetics. Importantly, the fact that our self-propelled simulated swimmers exhibit the same steady speeds as those observed in the experiments with live fish (to within 11%) provides an additional indication of the validity of the simulations presented here. We reiterate that an important consideration in the energetics comparisons in section 3.4 is the fact that the HT-/MT-continuous modes are extrapolations of realistic continuous-swimming behavior observed at higher speeds to slower speeds, which is necessary since the tetra fish did not exhibit continuous-swimming at low speeds. These kinematics were obtained by artificially expanding the time intervals between frames from high speed continuous swimming, which resulted in considerably smoother lateral undulations compared to the abrupt burst-coast motion, which in turn leads to markedly lower power requirement.

In conclusion, we demonstrate that improved energy-efficiency is not a primary outcome of burst-and-coast swimming in rummy nosed tetra fish. The higher energetic cost of burst-coast swimming when using experiment-based kinematics suggests that the primary purpose of intermittent swimming may instead be related to a combination of other functional aspects such as improved sensing and the likely existence of a minimum tail-beat frequency. Importantly, using sinusoidal traveling waves to generate idealized intermittent and continuous kinematics, instead of using experiment-based kinematics, results in comparable power requirements for the two swimming modes. Thus, it is feasible that appropriately optimized idealized burst-coast kinematics could be more energy-efficient than idealized continuous swimming.

Acknowledgment

SV acknowledges access to computational resources provided by Prof. Petros Koumoutsakos. The simulations were run at the Swiss National Supercomputing Center (CSCS) under project ID 's929'.

Appendix A. Swimmer shape

The body-geometry used in the simulations represents a simplified model of fish and is comprised of elliptical cross sections. The half-width $w(s)$ and half-height $h(s)$ of the elliptical cross sections are parametrized using two distinct natural cubic splines. These splines consist of 10 piecewise sections for $w(s)$ and 14 piecewise sections for $h(s)$. Here, s represents the curvilinear coordinate along the midline, starting at the head and terminating at the tail end. The knots and polynomial coefficients used for computing the half-width $w(s)$ are:

$$(s_0, \cdots s_i, \ldots, s_{10})/L = (0, 0.005, 0.01, 0.05, 0.1, 0.2, 0.4, 0.6, 0.8, 0.95, 1.0) \tag{15a}$$

$$a_{i,j} = \begin{pmatrix} 0.001\,5713 & 2.6439 & 0 & -15410 \\ 0.012\,865 & 1.4882 & -231.15 & 15598 \\ 0.016\,476 & 0.346\,47 & 2.8156 & -39.328 \\ 0.032\,323 & 0.382\,94 & -1.9038 & 0.7411 \\ 0.046\,803 & 0.198\,12 & -1.7926 & 5.4876 \\ 0.054\,176 & 0.004\,2136 & -0.146\,38 & 0.077\,447 \\ 0.049\,783 & -0.045\,043 & -0.099\,907 & -0.125\,99 \\ 0.035\,77 & -0.100\,12 & -0.1755 & 0.620\,19 \\ 0.013\,687 & -0.0959 & 0.196\,62 & 0.823\,41 \\ 0.006\,5049 & 0.0186\,65 & 0.567\,15 & -3.781 \end{pmatrix} \tag{15b}$$

Similarly, the knots and polynomial coefficients for the half-height $h(s)$ are:

$$(s_0, \cdots s_i, \ldots, s_{14})/L = (0, 0.01, 0.05, 0.1, 0.3, 0.5, 0.7, 0.8, 0.85, 0.87, 0.9, 0.993, 0.996, 0.998, 1) \tag{16a}$$

$$b_{i,j} = \begin{pmatrix} 0.001\,1746 & 1.345 & 2.2204e-14 & -578.62 \\ 0.014\,046 & 1.1715 & -17.359 & 128.6 \\ 0.041\,361 & 0.400\,04 & -1.9268 & 9.7029 \\ 0.057\,759 & 0.280\,13 & -0.471\,41 & -0.081\,02 \\ 0.094\,281 & 0.081\,843 & -0.520\,02 & -0.765\,11 \\ 0.083\,728 & -0.217\,98 & -0.979\,09 & 3.9699 \\ 0.032\,727 & -0.133\,23 & 1.4028 & 2.5693 \\ 0.036\,002 & 0.224\,41 & 2.1736 & -13.194 \\ 0.051\,007 & 0.342\,82 & 0.194\,46 & 16.642 \\ 0.058\,075 & 0.370\,57 & 1.193 & -17.944 \\ 0.069\,781 & 0.3937 & -0.421\,96 & -29.388 \\ 0.079\,107 & -0.447\,31 & -8.6211 & -1.8283e+05 \\ 0.072\,751 & -5.4355 & -1654.1 & -2.9121e+05 \\ 0.052\,934 & -15.546 & -3401.4 & 5.6689e+05 \end{pmatrix} \tag{16b}$$

Here, subscript i denotes the piecewise polynomial segment between knots s_{i-1} and s_i. The corresponding cubic polynomial describing the body half-width and half-height in each section may be reconstructed using the respective polynomial coefficients, as follows:

$$w_i(s) = L \cdot \left(a_{i,1} + a_{i,2}\,(s - s_{i-1})/L + a_{i,3}(s - s_{i-1})^2/L^2 + a_{i,4}(s - s_{i-1})^3/L^3\right) \tag{17}$$

$$h_i(s) = L \cdot \left(b_{i,1} + b_{i,2}\,(s - s_{i-1})/L + b_{i,3}(s - s_{i-1})^2/L^2 + b_{i,4}(s - s_{i-1})^3/L^3\right) \tag{18}$$

Appendix B. Swimming kinematics

The 3D Navier–Stokes simulations of burst-coast swimming are conducted using the swimming kinematics recorded from the experiments. We note that the only motion imposed on the fish models is the undulation of the midline; the forward- and rotational-motion of the swimmer are outcomes of the simulations due to flow-structure interaction between the undulating body and the surrounding fluid. We emphasize that the simulations are conducted in a free-swimming setup, as opposed to holding the swimmer stationary and imposing an inflow. This setup is a natural representation of actual fish swimming, and eliminates the need for tuning the inflow velocity or the kinematics to attain zero net force at steady state.

The midline kinematics used in the simulations were divided into three stages: the initial stage, where the fish starts from rest and utilizes undulatory motion described by an analytical travelling-wave; the final stage, where the midline motion is imposed from measurements extracted from the experimental videos; and an intermediate stage where the kinematics transition smoothly between the two stages using linear interpolation. This allows the fish to attain a steady swimming speed before switching over kinematics to the experimental-measurements and reaching the final steady state. The resulting initial-, transitional-, and final-stages can be observed in figures 4 and 5(c), as well as in supplementary movies 2 to 4.

The analytical sinusoidal travelling wave describing the lateral displacement of the midline (in the center-of-mass reference frame) during the initial stage is given as follows:

$$y(s) = \frac{4}{33} * (s + 0.031\,25L) * \sin\left(2\pi\left(\frac{s/L}{\lambda} - \frac{t}{T}\right)\right) \tag{19}$$

Here t represents time and T is the time period of undulations. The corresponding $x(s)$ coordinate is determined using the constraint that the distance between discretization points (ds) along the midline cannot change with time, since the fish length must remain constant during swimming. During the transitional stage, a linear interpolation is used to first decrease the analytical lateral displacement to zero, and then increase it to the experimentally-determined midline shape.

ORCID iDs

Intesaaf Ashraf https://orcid.org/0000-0002-1405-3803
Sam Van Wassenbergh https://orcid.org/0000-0001-5746-4621
Siddhartha Verma https://orcid.org/0000-0002-8941-0633

References

[1] Gleiss A C *et al* 2011 Convergent evolution in locomotory patterns of flying and swimming animals *Nat. Commun.* **2** 352

[2] Fish F E, Fegely J F and Xanthopoulos C J 1991 Burst-and-coast swimming in schooling fish (*Notemigonus crysoleucas*) with implications for energy economy *Comp. Biochem. Physiol. Physiol.* **100** 633–7

[3] Kramer D L and McLaughlin R L 2001 The behavioral ecology of intermittent locomotion *Am. Zool.* **41** 137–53

[4] Fuiman L A and Webb P W 1988 Ontogeny of routine swimming activity and performance in zebra danios (*Teleostei*: *Cyprinidae*) *Anim. Behav.* **36** 250–61

[5] Teyke T 1985 Collision with and avoidance of obstacles by blind cave fishAnoptichthys jordani (*Characidae*) *J. Comp. Physiol.* **157** 837–43

[6] Windsor S P, Tan D and Montgomery J C 2008 Swimming kinematics and hydrodynamic imaging in the blind mexican cave fish (*Astyanax fasciatus*) *J. Exp. Biol.* **211** 2950–9

[7] Santacruz A, Garcia O M, Tinoco-Cuellar M, Rangel-Huerta E and Maldonado E 2018 Spatial mapping in perpetual darkness: evo-devo of behavior in astyanax mexicanus cavefish *Biology and Evolution of the Mexican Cavefish* ed A C Keene, M Yoshizawa and S E McGaugh (Amsterdam: Elsevier) Ch 18 pp 361–76

[8] Mogdans J 2019 Sensory ecology of the fish lateral-line system: morphological and physiological adaptations for the perception of hydrodynamic stimuli *J. Fish. Biol.* **95** 53–72

[9] Dijkgraaf S 1963 The functioning and significance of the lateral-line organs *Biol. Rev.* **38** 51–105

[10] von Campenhausen C, Riess I and Weissert R 1981 Detection of stationary objects by the blind cave fishAnoptichthys jordani (*Characidae*) *J. Comp. Physiol.* **143** 369–74

[11] Wieskotten S, Dehnhardt G, Mauck B, Miersch L and Hanke W 2010 Hydrodynamic determination of the moving direction of an artificial fin by a harbour seal (*Phoca vitulina*) *J. Exp. Biol.* **213** 2194–200

[12] Weihs D 1974 Energetic advantages of burst swimming of fish *J. Theor. Biol.* **48** 215–29

[13] Videler J and Weihs D 1982 Energetic advantages of burst-and-coast swimming of fish at high speeds *J. Exp. Biol.* **97** 169–78 (https://jeb.biologists.org/content/97/1/169)

[14] Blake R W 1983 Functional design and burst-and-coast swimming in fishes *Can. J. Zool.* **61** 2491–4

[15] Floryan D, Van Buren T and Smits A J 2017 Forces and energetics of intermittent swimming *Acta Mech. Sin.* **33** 725–32

[16] Akoz E, Han P, Liu G, Dong H and Moored K W 2019 Large-amplitude intermittent swimming in viscous and inviscid flows *AIAA J.* **57** 3678–85

[17] Chung M-H 2009 On burst-and-coast swimming performance in fish-like locomotion *Bioinspir. Biomim.* **4** 036001

[18] Dai L, He G, Zhang X and Zhang X 2018 Intermittent locomotion of a fish-like swimmer driven by passive elastic mechanism *Bioinspir. Biomim.* **13** 056011

[19] Wu G, Yang Y and Zeng L 2007 Kinematics, hydrodynamics and energetic advantages of burst-and-coast swimming of koi carps (*Cyprinus carpio* koi) *J. Exp. Biol.* **210** 2181–91

[20] Müller U, Stamhuis E and Videler J 2000 Hydrodynamics of unsteady fish swimming and the effects of body size: comparing the flow fields of fish larvae and adults *J. Exp. Biol.* **203** 193–206 https://jeb.biologists.org/content/203/2/193

[21] McHenry M J and Lauder G V 2005 The mechanical scaling of coasting in zebrafish (*Danio rerio*) *J. Exp. Biol.* **208** 2289–301

[22] Tudorache C, Viaenen P, Blust R and De Boeck G 2007 Longer flumes increase critical swimming speeds by increasing burst-glide swimming duration in carp *Cyprinus carpio*, L. *J. Fish. Biol.* **71** 1630–8

[23] Webb P W 1984 Form and function in fish swimming *Sci. Am.* **251** 72–82

[24] Webb P W 1994 The biology of fish swimming *The Mechanics and Physiology of Animal Swimming* ed L Maddock, Q Bone and J M V Rayner (Cambridge: Cambridge University Press) pp 45–62

[25] Ashraf I, Godoy-Diana R, Halloy J, Collignon B and Thiria B 2016 Synchronization and collective swimming patterns in fish (*Hemigrammus bleheri*) *J. R. Soc. Interface* **13** 20160734

[26] Ashraf I, Bradshaw H, Ha T-T, Halloy J, Godoy-Diana R and Thiria B 2017 Simple phalanx pattern leads to energy saving in cohesive fish schooling *Proc. Natl Acad. Sci. USA* **114** 9599–604

[27] Ashraf I 2018 Interactions in collective fish swimming *PhD Thesis* Sorbonne Paris Cité

[28] Li G *et al* 2020 Burst-and-coast swimmers optimize gait by adapting unique intrinsic cycle (arXiv:2002.09176)

[29] Angot P, Bruneau C-H and Fabrie P 1999 A penalization method to take into account obstacles in incompressible viscous flows *Numer. Math.* **81** 497–520

[30] Chorin A J 1968 Numerical solution of the Navier–Stokes equations *Math. Comput.* **22** 745

[31] Rossinelli D *et al* 2013 11 pflop/s simulations of cloud cavitation collapse *SC'13: Proc. of the Int. Conf. on High Performance Computing, Networking, Storage and Analysis* (IEEE) pp 1–13

[32] Verma S, Novati G and Koumoutsakos P 2018 Efficient collective swimming by harnessing vortices through deep reinforcement learning *Proc. Natl Acad. Sci. USA* **115** 5849–54

[33] Novati G, Verma S, Alexeev D, Rossinelli D, van Rees W M and Koumoutsakos P 2017 Synchronisation through learning for two self-propelled swimmers *Bioinspir. Biomim.* **12** 036001

[34] Tytell E D and Lauder G V 2004 The hydrodynamics of eel swimming: I. wake structure *J. Exp. Biol.* **207** 1825–41

[35] Verma S, Hadjidoukas P, Wirth P and Koumoutsakos P 2017 Multi-objective optimization of artificial swimmers *Congress on Evolutionary Computation (CEC)* (IEEE) pp 1037–46

[36] Bainbridge R 1958 The speed of swimming of fish as related to size and to the frequency and amplitude of the tail beat *J. Exp. Biol.* **35** 109–33 (https://jeb.biologists.org/content/35/1/109)

[37] Hunter J R and Zweifel J R 1971 Swimming speed, tail beat frequency, tail beat amplitude, and size in jackmackerel, *Trachurus symmetricus*, and other fishes *Fish. Bull.* **69** 253–66

[38] Verma S, Papadimitriou C, Lüthen N, Arampatzis G and Koumoutsakos P 2020 Optimal sensor placement for artificial swimmers *J. Fluid Mech.* **884** A24